

Lymphocytes can self-steer passively with wind vane uropods

Authors: Marie-Pierre Valignat^{1,2,3}, Paulin Nègre^{1,2,3,4}, Sophie Cadra^{1,2,3}, Annemarie C. Lellouch^{1,2,3}, François Gallet⁵, Sylvie Hénon⁵, and Olivier Theodoly^{1,2,3*}

¹Aix Marseille Université, LAI UM 61, Marseille, F-13288, France.

²Inserm, UMR_S 1067, Marseille, F-13288, France.

³CNRS, UMR 7333, Marseille, F-13288, France.

⁴APHM, Hôpital de la Conception, Laboratoire d'Immunologie, Marseille, F-13385, France.

⁵ Université Paris-Diderot, CNRS, MSC UMR 7057, Paris, F-75205, France.

*Correspondence to: Olivier.theodoly@inserm.fr

Abstract

A wide variety of cells migrate directionally in response to chemical or mechanical cues, however the mechanisms involved in cue detection and translation into directed movement are debatable. Here, we investigate a model of lymphocyte migration on the inner surface of blood vessels. Cells orient their migration against fluid flow, suggesting the existence of an adaptive mechano-transduction mechanism. We find that flow detection may not require molecular mechano-sensors of shear stress and detection of flow direction can be achieved by the orientation in the flow of the non-adherent cell rear, the uropod. Uropods act as microscopic wind vanes that can transmit detection of flow direction into cell steering via the on-going machinery of polarity maintenance, without need for novel internal guidance signalling triggered by flow. Contrary to chemotaxis, which implies active regulation of cue-dependant signalling, upstream flow mechanotaxis of lymphocytes may only rely on a passive self-steering mechanism.

Introduction

Cell migration plays an essential role in the living world, from nutrient searching in mono-cellular organisms, to morphogenesis, tissue repair, and immune cells patrolling in multi-cellular organisms. To perform such complex tasks efficiently, cells are frequently guided toward targeted locations by various external cues such as soluble chemicals (chemotaxis), surface-bound chemicals (haptotaxis), or mechanical stimuli like substrate stiffness, cell deformation or hydrodynamic stress (mechanotaxis). Guiding mechanisms have long been studied and yet many aspects of these sophisticated processes remain unexplained. We are interested here in the recently observed phenomenon of leukocyte guidance by a hydrodynamic flow. Before extravasation from the blood stream into tissues, circulating leukocytes arrest and crawl with an amoeboid motility¹ on the luminal surface of blood vessels under the influence of an intense shear stress exerted by flowing blood. The role of flow on leukocyte crawling and extravasation remains generally an unsolved question², however crawling T lymphocytes were recently reported *in vivo*³ and *in vitro*⁴ to orient *against* the direction of flow and to move upstream like salmon in a river. This non-intuitive behaviour is manifestly not a *drift* of cells pushed by the flow, and we sought here to clarify the origin, role and mechanism of this upstream flow mechanotactic behaviour.

Eukaryotic chemotaxis is the most prominent and studied guidance mechanism. Signal detection by cells exposed to a soluble chemical gradient occurs via known molecular sensors (G-protein coupled receptors) that are specific for various factors. They are usually distributed fairly evenly on the cell surface^{5,6} and produce a differential outside/inside signalling between the front and rear of cells (Fig. 1a). A complex signalling pathway eventually yields a polarized phenotype with biased motility toward the gradient⁷. In comparison, the deciphering of mechanotaxis is much less advanced. Relatively few molecules have been identified as potential mechanical sensors, for instance the Src kinase substrate p130Cas, which is phosphorylated under an extension force⁸. As adaptive phosphorylation of p130Cas was reported to be involved in the downstream orientation of endothelial cells⁹, one may imagine an active mechanism analogous to chemotaxis for flow mechanotaxis, involving local molecular sensing of external cues and specific internal signalling to reorient migration. Yet, a critical consideration is that while chemical concentration and substrate rigidity in chemotaxis and mechanotaxis respectively are gradient signals, the hydrodynamic shear stress in flow mechanotaxis is homogeneous in the plane of cellular displacement. A chemotaxis-analogue scenario with molecular force sensors homogeneously distributed would therefore yield a non polarized internal signalling and no directional sensing (Fig. 1b). A polarized repartition of molecular sensor (Fig. 1c) or cell morphology (Fig. 1d), could generate a differential rear-front signalling under homogeneous stress. However, the existing polarization axis would be enhanced under flow but would not depend on the direction of flow. Flow mechanotaxis seems therefore intrinsically incompatible with a local detection by molecular sensors of force only, which suggests that a structural organization at the supramolecular⁹ or cellular level is required. The location and the type of detection involved in the flow depended migration of T lymphocytes remain therefore unclear.

Herein, we analyzed the mechanism of T lymphocyte guidance under flow using microfluidic devices to impose changes of flow direction and magnetic beads to exert localized forces on the cell body. We show that detection of flow direction when lymphocytes crawl against the flow is achieved at the organelle level by the cell rear, or uropod, that orients in the flow like a wind vane. Singularly, upstream migration was not hampered by inhibition of classical guidance signalling pathways and changes in the direction or intensity of flow did not trigger calcium signalling, which together challenge the relevance of an active guidance mechanism.

We show, however, that the maintenance of a single polarity axis with an aligned lamellipod and uropod can spontaneously induce cells to face the flow when their uropod orients like a wind vane. Given the intrinsic polarity of the T cells, this process can be characterized as passive steering since it is built on pre-existing polarity signalling structures that do not need to be induced by the flow or magnetic stimulus.

Results

Cells Uropods reorient with flow direction like a wind vane. We used primary human effector T lymphocytes on intercellular adhesion molecule 1 (ICAM-1) coated glass substrates as a minimal in vitro model system to study crawling orientation under flow (Fig. 2a). Without additional chemical or mechanical cue, these cells are polarized, adherent and spontaneously motile. An active lamellipod, which extends in the cell front, is considered to act as the motor of the migration machinery via actin polymerization¹⁰. The central body is mainly occupied by the nucleus and at the cell rear, the uropod is a characteristic organelle of T lymphocytes, whose role in cell migration remains enigmatic¹¹. In the absence of flow, crawling cells display a random motion with a velocity around $20 \mu\text{m}.\text{min}^{-1}$ and a persistence length around $50 \mu\text{m}$, whereas in a unidirectional flow corresponding to a shear stress of $10 \text{ dyn}.\text{cm}^{-2}$, all T lymphocytes orient their migration direction upstream (Fig. 2b). The total shear force on the cells ($\sim 100 \text{ pN}$ at $10 \text{ dyn}.\text{cm}^{-2}$) is known to be negligible as compared to the force developed by the powerful motility machinery in the lamellipod ($> 1000 \text{ pN}$)⁴. This has previously permitted us to explain why cell velocity remains unaffected by flow⁴, but it also supports the idea that migration orientation is a specific adaptation of lymphocytes to the relatively faint hydrodynamic cue. However, it is unknown whether this adaptation is active or passive, nor whether it arises from the cell front (lamellipod) or cell rear (uropod). For instance, polarized cells are commonly described as being more sensitive to chemoattractant at the anterior than at the posterior⁵. Recent microfluidics experiments on neutrophil chemotaxis show indeed that a cell engages a turn when its leading edge only is exposed to a 90° change of chemical cue direction¹². Similarly, we used a microfluidic chamber to expose lymphocytes to a 90° change in flow direction (Fig. 2c and Supplementary Movies 1 and 2). Initially, crawling cells project lamellipods towards the flow and uropods are elongated in their wake. When flow direction changes, the lamellipods growth keeps its original orientation, whereas most uropods are instantaneously pushed sideways or even aligned by the flow of new direction. This observation strongly suggests that uropods may play a leading role in the adaptation of the migration to flow direction.

Uropods can rotate with flow due to their non adherence. We therefore characterized further the properties of a uropod within its microenvironment. Firstly, the conformation of effector T lymphocytes above the substrates was imaged by confocal microscopy (Fig. 3a and Supplementary Movie 3), and shows that a uropod protrudes typically $10 \mu\text{m}$ above the surface in absence of flow. Considering the uropod as a vertical cylinder, the force of the flow on the uropod, F_u , can be estimated¹³ by $F_u = \int_0^L \frac{4\pi\mu}{2 - \ln(\rho V(z)/\mu R)} V(z) dz$, where z is the height above the surface, μ and ρ are the medium viscosity and density, R the radius of the cylinder, and $V(z)$ is the fluid velocity at height z . A shear stress $\sigma = 10 \text{ dyn}.\text{cm}^{-2}$, a uropod length $L = 10 \mu\text{m}$ and a radius $R = 2 \mu\text{m}$ yield a force $F_u \approx 100 \text{ pN}$. Thus, the hydrodynamic force on the uropod alone is of the same magnitude as that exerted on the whole cell considered as flat, $F_c = S_p \sigma$, with $S_p \approx 100 \mu\text{m}^2$ the projected area of individual cells. Indeed fluid velocity at a blood vessel surface is null - according to classical hydrodynamic condition

of no-slip at solid surface - and increases linearly away from the surface. The erected uropods expose their extremity to higher fluid velocities, which amplifies the force experienced by cell rear for a given flow condition. Secondly, the footprint of the cell on the substrate was imaged by reflection interference contrast microscopy (RICM) (Fig. 3b and Supplementary Movie 4). The lamellipod and the central cell body were found to be in close contact with the surface, whereas the uropod was clearly non adherent. Comparison with total internal reflection fluorescence microscopy (TIRF) images (Fig. 3c) shows that the footprint zone seen in RICM coincides with the presence of integrins. This latter observation is consistent with previous reports of T cell crawling showing that adhesion and migration properties are mediated by integrin/ICAM binding and affinity regulation in the front and central body¹⁴. In contrast, the former observation of non-adherence of the cell rear is surprising relative to existing paradigms on cell motility: for mesenchymatous cells, cell rear is clearly adherent and requires strong acto-myosin traction to detach¹⁵, and for amoeboid cells, actomyosin traction is also reported to be concentrated in uropods¹⁶. Nevertheless, the non-adherence of lymphocytes uropods is directly relevant for flow-guided migration, as it allows the fast rotation and orientation of uropods with flow in the plane of the substrate, like for a free-rotating wind vane (Supplementary Note 1 and Supplementary Fig. 1). In the end, prominence and most importantly non-adherence make uropods sensitive organelles for detection of flow *direction*.

Cell motility direction is opposed to uropod orientation. The question remains whether uropods can then transduce their orientation with the flow into a directional cue for migration of cells. We therefore performed a series of experiments to demonstrate that flow guidance arises from the posterior of the cells. We first attached anti-ICAM-3 labelled micron-sized beads on the uropod of T lymphocytes, where adhesion molecule ICAM-3 is specifically enriched. When exposed to flow, the cells with beads on their uropod migrate upstream like normal cells without beads, whereas cells attached in multiplets to a common bead have an orientation clearly independent of flow (Fig. 3d and Supplementary Movie 5). In fact, cell multiplets form quasi-stable patterns with an immobile “cross-linking” point at the center and cells pulling radially in diverging directions with regular angles between cells. The independence of orientation with flow is consistent with the fact that mutual tractions between cells induced by their powerful motility machinery overcome the hydrodynamic shear stress on each cell⁴. Moreover, according to Newton’s law, the sum of forces on the immobile bead of a multiplet is null at equilibrium, and considering that each cell roughly develops the same force and pulls away from its uropod, multiplets of n cells are expected to form regular star patterns with angles between branches of $2\pi/n$. The static behaviour of multiplet suggests therefore that it is not directly the flow direction but rather the position of the uropod that is determinant for a cell forward orientation. The dynamic role of uropod on cell orientation can then be observed with cells escaping unstable positions. In Fig. 3e and Supplementary Movie 6, the cell trailing edge is trapped on a surface defect, and cell orientation is opposite to the attachment point, like in a multiplet. The flow is orientated from right to left in opposition to cell orientation, so that the cell is initially 180° apart from its equilibrated upstream-bound orientation. When the attachment point breaks, the uropod immediately initiates a repositioning downstream of the cell, and the cell resumes a normal upstream crawling within 100 s. Hence, if the hydrodynamic stimulation is insignificant compared to the powerful cell motility machinery to directly alter the velocity and orientation of a crawling cell, it easily orients the free-rotating uropod downstream of a cell body, which then manifestly triggers the reorientation of the whole cell. Uropods seemingly act like a wind vane that can direct cells direction.

Uropod deflection controls steering of cells. To challenge the role of uropod as a wind vane-type regulator of cell migration direction, we then quantified the external stimulus required to actuate the guidance mechanism. In a first experiment, we attached large beads of 12 μm diameter to the cells' uropod to amplify the hydrodynamic drag on the cell rear. Cells equipped with such amplifiers are expected to be more sensitive to surrounding flow conditions. Cell velocity is not dependant of bead presence (Supplementary Note 2 and Supplementary Fig. 2), whereas upstream orientation is indeed systematically more pronounced as compared to control cells (Fig. 4a). Considering that the size of the cell rear is dominated by the size of the bead, and that beads under flow are pushed in contact to the surface, the hydrodynamic drag force, F_d , on the cell rear can be estimated by the force on a sphere settling on a flat surface and submitted to a flow, $F_d \approx 32 a^2 \sigma$, where a is the diameter of the bead and σ the local shear stress¹⁷. The onset of orientation versus flow corresponds to a force on the bead of approximately 30 pN. This range of force is accessible with magnetic actuation of beads. We therefore equipped cells with magnetic beads on their uropod, and exposed them to a permanent magnet. As compared to flow experiments, mechanical actuation applies here only on the uropod and not on the whole cell body. In these conditions, cells orient their path in the opposite direction to the magnetic force (Fig. 4b). Hence, whether by flow or magnetic actuation, the uropod acts as a steering-wheel of the "crawling cell" vehicle. By actuating this steering-wheel, one can navigate individual lymphocytes like radio-controlled toys, as in the experiment of Fig. 4c and Supplementary Movie 7. The distance between the cell equipped with a magnetic bead and the tip of a magnetic tweezers is here maintained constant via a dynamic control of the microscopic stage, and sequential applications of hydrodynamic and magnetic forces making an angle of 90° allows one to drive lymphocytes on a step-like pathway.

Upstream crawling works without usual guidance signalling. If the uropod-wind vane detects flow direction and guides cells, it remains unclear how the transmission of cue detection into a steering command to the whole cell is performed. The existence of a specific internal signalling triggered by cue detection has been tested by visualizing intracellular calcium levels changes using fluo4 PBX labelling (Fig. 5a and Supplementary Movie 8). Clearly, interactions between the uropod and flow trigger no change in calcium concentration. Since calcium is involved in many signalling pathways, these data challenge the existence of an active transmission between cue detection and directivity. Furthermore, high affinity integrins and/or calcium channels have been reported as key element in the active mechanism of neutrophils recruitment and guidance^{18,19}. However, with effector T lymphocytes, we found that inhibitors of calcium-release-activated (CRAC) channels (Supplementary Note 3 and Fig. 3), as well as promoters of either integrins high or low affinity states had a weak effect on crawling speed and direction, in the presence and in the absence of external flow (Supplementary Note 4 and Supplementary Fig. 4). Finally, Phosphoinositide 3-kinases PI(3)Ks play an important role in the active gradient sensing signalling machinery in chemotaxis of amoebae *Dictyostelium*^{20,21}, and was also reported to be involved in galvanotaxis of keratocytes²² and mechanotaxis of *Dictyostelium Discoideum*²³, *Entamoeba Histolytica*²⁴ and endothelial cells²⁵. However, inhibitors of PI(3)Ks or G protein coupled receptors (Supplementary Note 5 and Supplementary Fig. 5) hardly affect migration and upstream mechanotaxy of effector T cells. Altogether, these data show that common intracellular guidance signalling pathways involved in various cell guiding mechanisms are not involved in upstream mechanotaxis of effector T lymphocytes. This supports exploration of alternative mechanisms for transmission between cue detection and cell direction.

Cells can navigate under passive wind vane self-steering. A maritime analogy allows us to propose a minimal and plausible model of guiding mechanism for lymphocytes, which requires no unknown signalling to transduce cue detection into motility machinery remodelling. Sailors have used passive mechanical wind vane self-steering gears (Fig. 5b) to navigate single-handed on sailing boats^{26,27}, long before the advent of active electronic self-steering systems guided by compass or GPS signals. In the functioning of wind vane self-steering gears, a wind vane is adjusted to face into the wind when the boat is on the right course. When the boat wanders off course, the wind strikes the wind vane from one side and the slight rotation of the wind vane by the faint wind force biases a steering system (a steering wheel or a trim-tab on the rudder) that has sufficient power to reorient the boat (Fig. 5c). Similarly, the uropod of lymphocytes has a wind vane behaviour that is sensitive to faint flows. The change of uropod-wind vane orientation biases directly the rear-front axis of cell polarization (Fig. 5c) and the robust mechanism of polarization maintenance can then trigger cell steering by re-establishing the lamellipod/uropod alignment. In this view, there is no activation of a specific internal signalling cascade by specialized sensors, like in chemotaxis. The internal regulation of rear-front polarization may remain unchanged with or without mechanical stimulation by flow, and cells will respond passively to the external solicitation with upstream phenotype.

Perturbation of the self-steering system by inhibitors. To test further the idea that the uropod/wind vane coupled to the on-going rear-front polarization regulation is the steering mechanism of lymphocytes flow mechanotaxis, we then applied drugs to perturb the main cogs of this machinery, first the transmission system (cell polarity) and then the detection system (cell uropod/wind vane). The uropod contains a microtubule network¹¹ that is known to participate in maintaining cell cortical polarity²⁸. Disruption of microtubules with nocodazole (Fig. 6a, Supplementary Movie 9) or vinblastin provoked frequent turning of cells, and diminished the average orientation of cells with flow (Fig. 6a,b, Supplementary Note 6 and Supplementary Fig. 6), consistent with previous observations on neutrophils²⁹ and lymphocytes³⁰. Perturbation of cell polarity by nocodazole is clearly revealed by the much wider shape of the lamellipod that tends to extend in 360° directions (Fig. 6c and Supplementary Movie 10). Within the model of the wind vane regulated self-steering, impairment of the rear-front polarization, i.e. of the transmission system of flow direction detection into steering command, is straightforwardly consistent with the observed loss of guidance with flow. We then treated cells with blebbistatin, a potent inhibitor of acto-myosin activity. Blebbistatin-treated cells present a strong elongation of their non-adherent uropods (Fig. 6c and Supplementary Movie 11) as previously observed³¹, and a marked increase of cell orientation with flow (Fig. 6b and Supplementary Movie 12). Adherence with the substrate is not responsible for uropod rearward elongation. The uropods of blebbistatin treated cells remain markedly non adherent, as revealed by images of the cells footprint on the substrate (Supplementary Movie 13) and by uropod instantaneous adaptation to changes in flow direction (Supplementary Movie 14). In fact, decrease of acto-myosin activity is known to diminish microvilli stability and promote membrane unfolding under stress³², which explains the elongation of uropods under flow. Within the model of the wind vane regulated self steering, a wind vane of larger size has a higher sensitivity to flow direction, which is consistent with the observed increase of guidance efficiency with flow. More quantitatively, we determined the average uropods length L_u for each experimental conditions and then plotted the directionality $\langle \cos \theta \rangle$ of cells treatment against $\sigma^* L_u^2$, which characterizes the strength of the torque to align the uropods (Fig. 6d). All data with and without blebbistatin follow a single master curve, which is consistent with the size of the uropod/wind vane being the main cause of guidance sensibility enhancement by blebbistatin treatment. Finally, we

found a net correlation between the time of persistence in absence of flow, as determined at the transition between the directional and diffusive regime yields (Fig. 2b), and the efficiency of the guidance by flow (Fig. 6e). This observation is in accordance with a guidance model relying on the properties of the polarization mechanism that are already in place in absence of flow.

Discussion

In the end, whereas chemotaxis is based on an active self-steering system (like electronic navigation device), with an external cue detected and specifically processed to activate guidance signalling and new functions at different locations in the cell, flow mechanotaxis can be explained by a passive self-steering system (like mechanical wind vane device), with only continually maintained polarity signalling and without new internal signalling specific to the external cue. This scenario is also consistent with the fact that active chemotaxis allows adaptation to increasing signals as cells travel up a gradient on four orders of magnitude⁶, whereas passive flow mechanotaxis is only efficient for a limited range of stimuli.

The physiological benefit of flow orientation is currently unknown for lymphocytes and more generally for neutrophils¹⁶, endothelial cells⁹ or amoebae²³. The fact that neutrophils crawl downstream¹⁶ and T lymphocytes upstream⁴ while migrating on the same adhesive ligand, challenges the idea of a universal flow guided mechanism selected to favour extravasation. Furthermore, as upstream crawling may not rely on a specific signalling mechanism, one cannot exclude that flow orientation may be a fortuitous consequence of uropod morphology. Nevertheless, the robust flow mechanotaxis behaviour of T lymphocytes supports the idea of a mechanism purposely selected by evolution. If evolution is not requisite to shape a passive mechanism, it may nevertheless play a direct role, for instance by tuning the morphology of the uropod that is the trigger of the mechanism. We may speculate that the evolutionary advantage of upstream crawling could be to guide lymphocytes toward the epicentre of signalling endothelial zone, if their arrest occurred downstream of the epicentre.

FIGURES

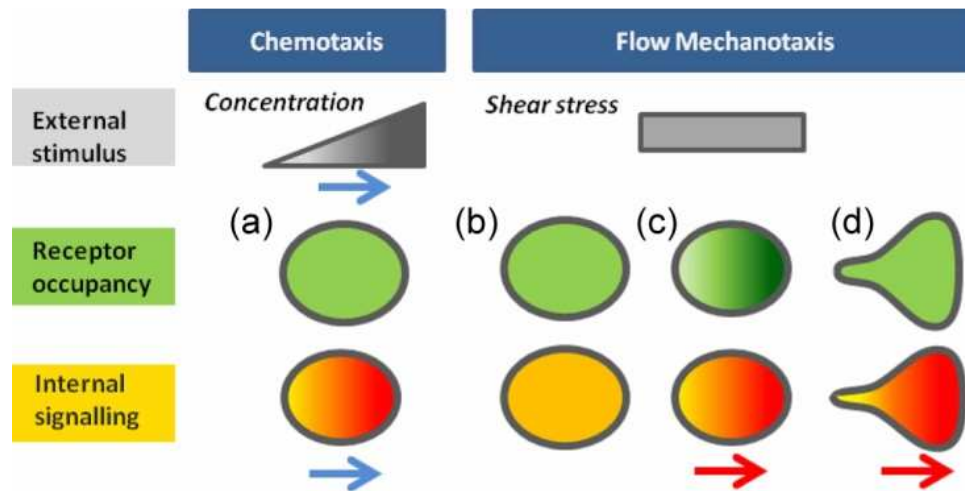


Fig. 1. From local detection of an external cue to global cellular guiding. Schematic mechanistic pictures for chemotaxis and flow mechanotaxis of the spatial variation of (grey) the external stimuli, (green) the molecular sensor distribution, and (orange) the cell internal signalling by molecular sensors. Darker colour stands for higher intensities. (a) In chemotaxis, the external cue is a gradient of bulk concentration. Local molecular sensors of concentration evenly distributed⁵ on cells induce internal polarized signalling in line with the direction of the gradient cue (Blue arrows). (b-d) In flow mechanotaxis, the external cue (shear stress) is homogeneous in the plane of displacement. In hypothetical models involving local molecular sensors of force, i.e. symmetric cell with homogenous (b) and inhomogeneous (c) sensor occupancy, and (d) asymmetric cell with homogeneous sensor occupation, the direction of internal signalling (red arrow) corresponds to a reinforcement of rear-front polarization that is independent of flow direction.

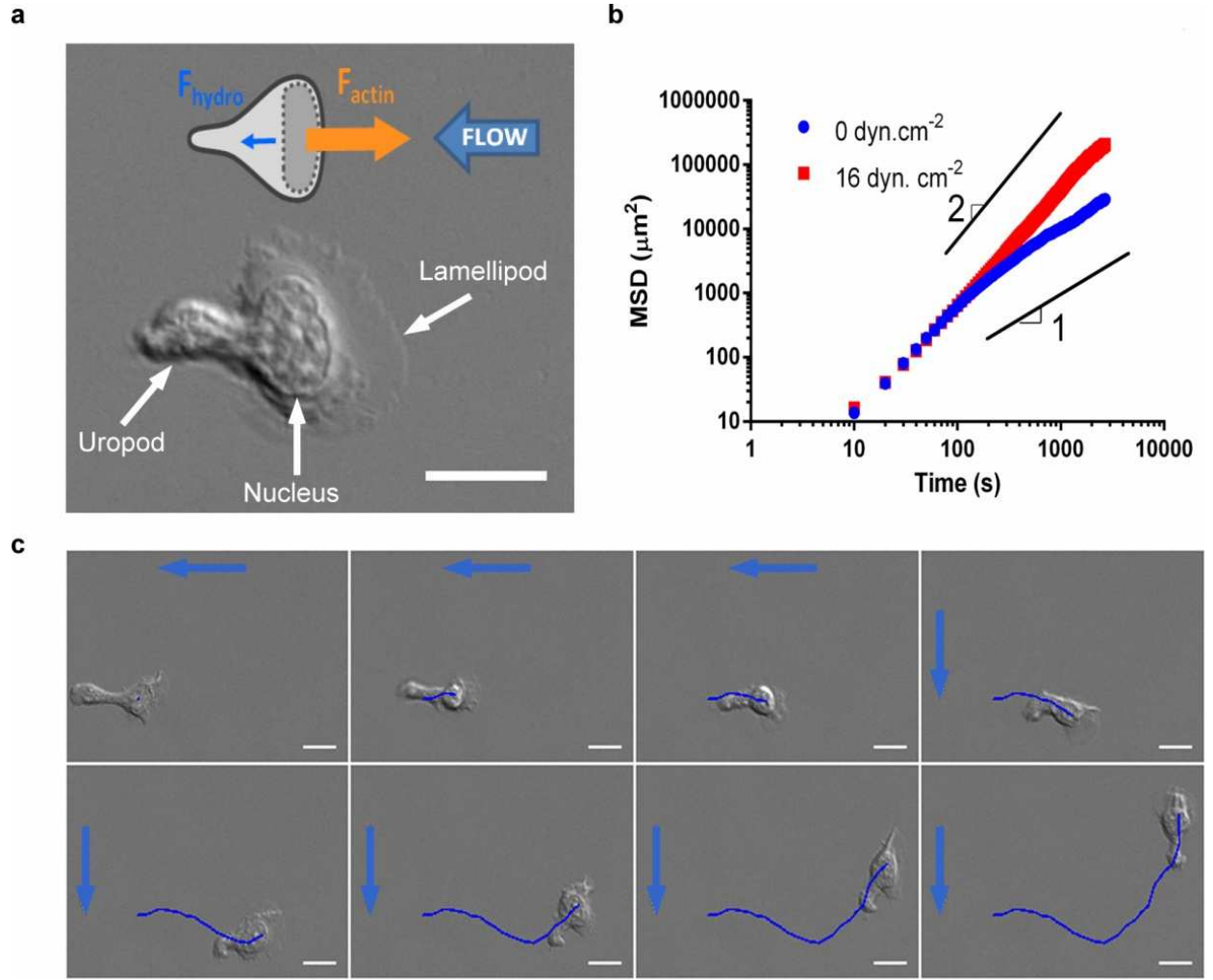


Fig. 2. Transition from diffusive to directional motility under flow and adaptation to changes of flow direction. (a) DIC image of a lymphocyte crawling on ICAM-1/BSA coated glass substrate with lamellipod in the front, nucleus in the centre and protruding uropod in the rear. Scale bare is 10 μm . Cartoon represents a crawling lymphocyte under flow with the faint hydrodynamic force F_{hydro} pushing to the left (blue arrow) and the strong internal force due to actin polymerization in the lamellipod F_{actin} pushing to the right (orange arrow). (b) Average Mean Square Displacement (MSD) of N_{cell} tracked cells as function of time lag in log-log scale. Blue plot: in absence of flow ($N_{cell}=541$), the long term behavior is almost diffusive (slope 1). Transition between directional and diffusive regime yields a persistence length of 50 μm . Red plot: under a shear stress of 16 dyn.cm^{-2} ($N_{cell}=650$), the long term behaviour is almost ballistic (slope 2). (c) Sequence of 8 images separated each by 200s of a crawling lymphocytes under a shear flow of 8 dyn.cm^{-2} with a flow (blue arrows) coming first from the right and then from the top (after $t = 156$ s). Dark blue line traces the track of the cell starting from the first image. Scale bar = 10 μm .

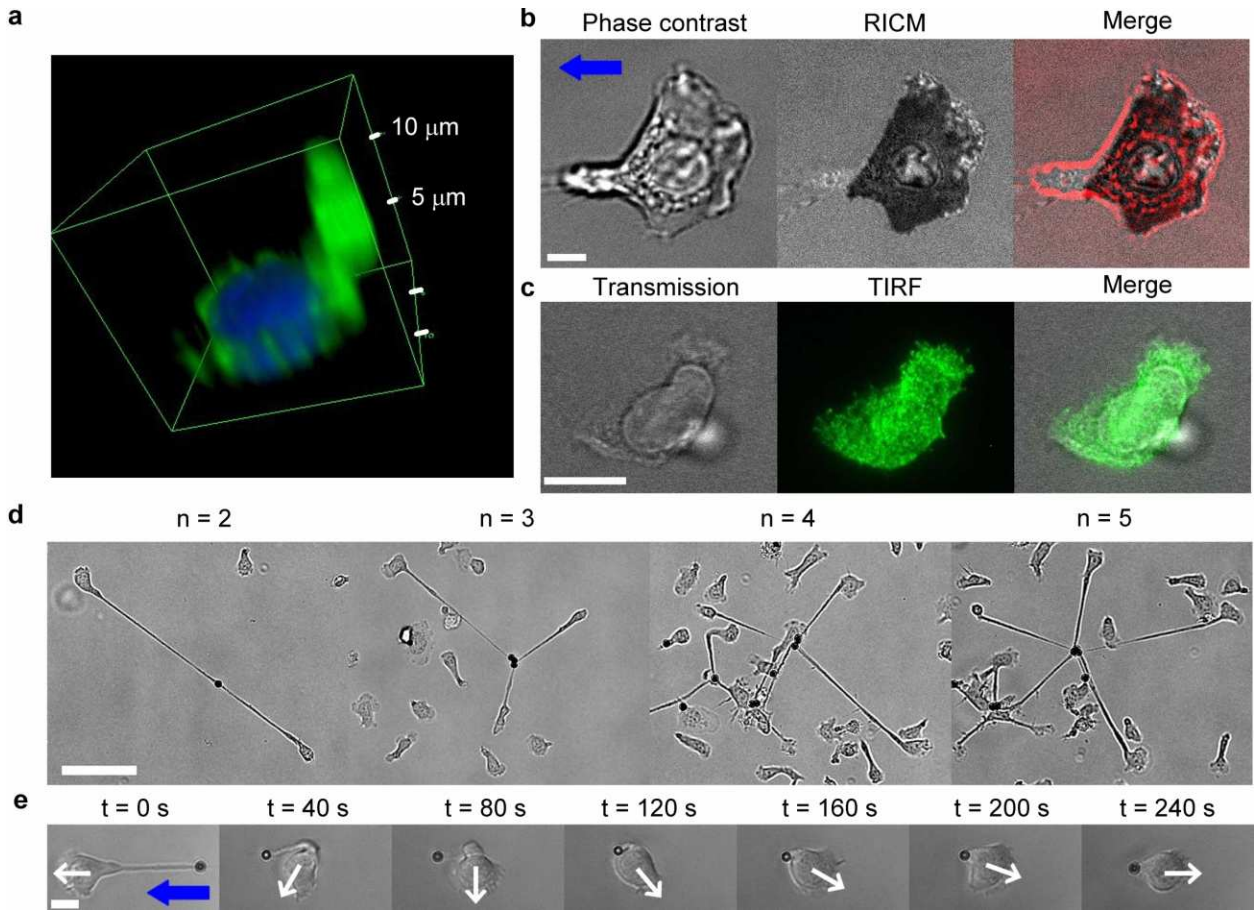


Fig. 3. Prominent and non-adherent uropods act as wind vanes in the flow and guide cells. (a) Confocal image of a T lymphocyte stained for the membrane (green) and the nucleus (blue) in the absence of flow. (b) T lymphocyte under a shear stress of 8 dyn.cm^{-2} in phase contrast (PC) mode, in RICM mode. Blue arrow indicates flow direction. Scale bar 5 μm . (c) Fixed T lymphocyte without flow and in presence of Ab38 against LFA-1 integrins (green) in transmission and TIRF mode. Scale bar = 10 μm . (d) Multiplets of T lymphocytes attached by their uropod to anti-ICAM3 coated beads with number of cells n per multiplet ranging between 2 and 5. Cells orientation in multiplets is independent of flow direction but multiplets of n cells take quasi-stable star-like conformations with regular angles of $2\pi/n$ between branches. Scale bar = 50 μm (e) Image sequence showing the dynamic reorientation of a T lymphocyte in a right to left flow (blue arrow) corresponding to a shear stress of 10 dyn.cm^{-2} . Initially, cell faces downstream due to an attachment of the trailing edge. After the link breaking ($t = 0$ s), it reorients progressively toward the flow. White arrows indicate the instantaneous lamellipod extension direction. Blue arrow indicates flow direction. Scale bar is = 10 μm .

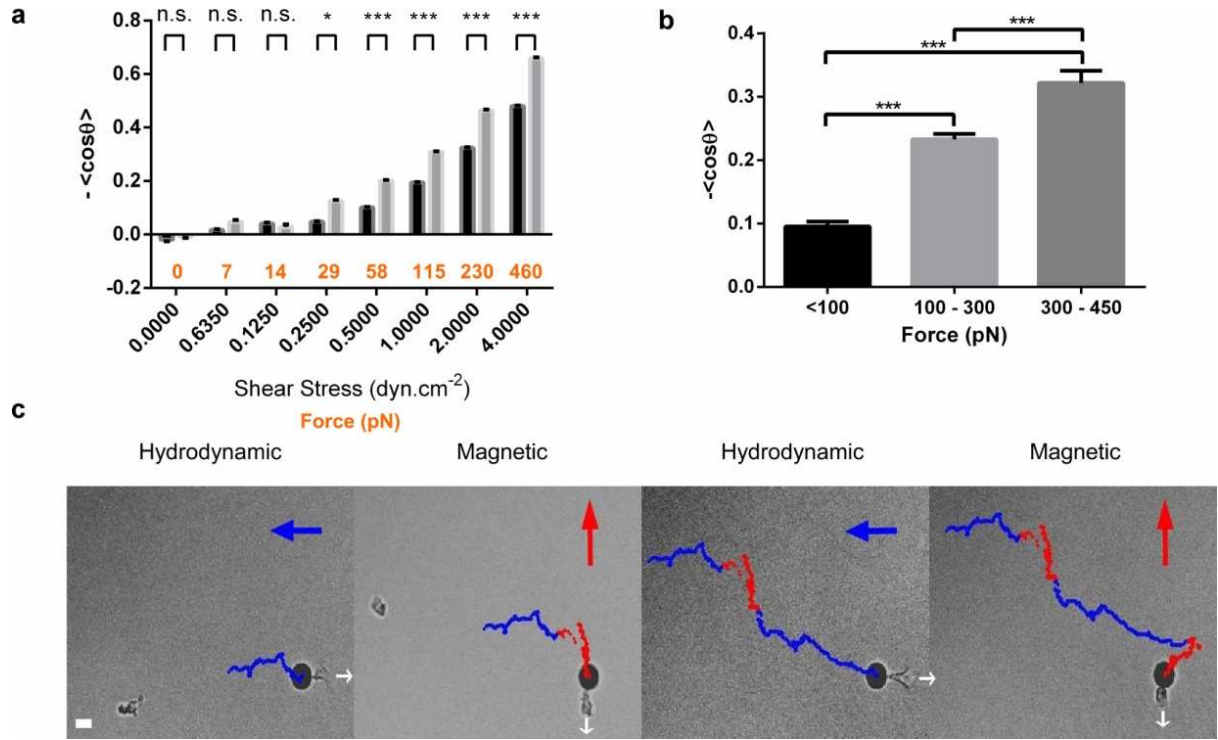


Fig. 4. Quantification of cell steering by uropod. (a) Index of directionality $\langle \cos \theta \rangle$ versus axis of flow direction as a function of shear stress intensity (black x-axis) for control lymphocytes (black bars) and lymphocytes with 12 μm diameter magnetic beads attached to cells uropods (grey bars). The force on the cell rear, F_r , exerted by the bead is indicated in orange on x-axis¹⁷. Data for each condition were calculated for more than 50 cells after four independent experiments. Error bars indicate \pm s.e.m. * $P < 0.05$, ** $P < 0.01$, *** $P < 0.001$ (two tailed unpaired t -test). (b) Index of directionality $\langle \cos \theta \rangle$ versus axis of magnetic gradient as a function of horizontal magnetic force exerted to the beads on the cells uropods. $N_{steps} > 20,000$. Data are mean \pm s.e.m. of three independent experiments. * $P < 0.05$, ** $P < 0.01$, *** $P < 0.001$ (one way ANOVA followed by the Tukey multiple-comparison test). (c) Driving a lymphocyte using the uropod as a steering-wheel. Sequence of images at times $t = 720$ s, $t = 1200$ s, $t = 2380$ s and $t = 3000$ s, of a single lymphocyte with a 12 μm diameter magnetic bead attached to its uropod and submitted alternatively to hydrodynamic force (blue arrow) pulling the bead to the left and to a magnetic force (red arrow) pulling the bead to the top. The cell is kept immobile in the field of view via a dynamic control of the microscope X-Y stage to maintain the distance between the bead and the magnetic tip constant. Dots indicate the successive relative positions of the cell every 2 s during hydrodynamic (blue dots) and magnetic (red dots) actuation. White arrows indicate cell polarization direction. The trajectory displays steps with blue horizontal segments and red vertical segments corresponding to the cycles of respectively hydrodynamic and magnetic actuation of 200 pN with 90° angle. Scale bar = 10 μm.

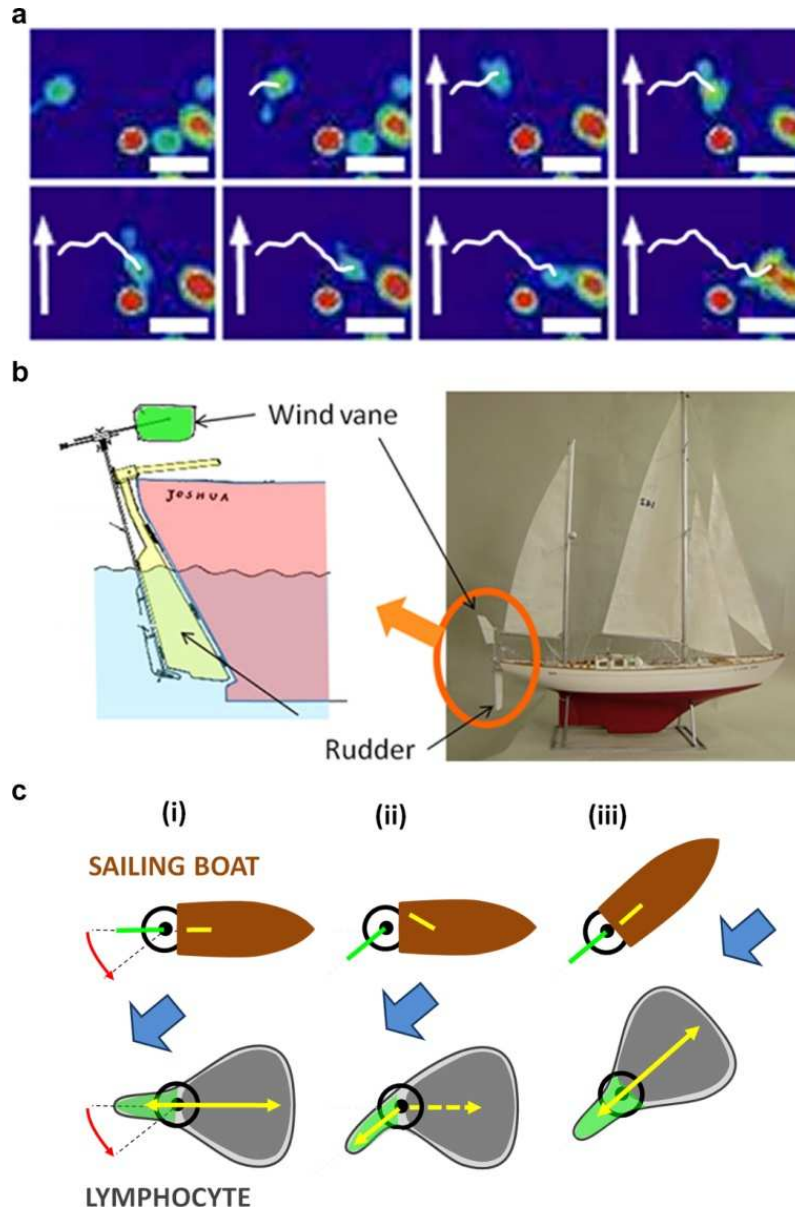


Fig. 5. Self-steering under passive uropod/wind vane regulation. (a) Flow triggers no internal calcium signalling. Sequence of images taken every 1 min of relative intracellular calcium levels in crawling lymphocytes under flow using fluo-4 PBX. Calcium sensor intensity is displayed with a pseudo-colour glow scale (red, highest to blue, lowest activity). Flow is null in the beginning, and a white arrow indicating flow direction appears when flow is started with a shear stress of 8 dyn.cm^{-2} . Calcium level is unaffected by flow application, but strongly increased upon cell encounters (last image). White line indicates the track of the migrating cell of interest. Scale bar = $20 \mu\text{m}$; sequence is representative of 10 cells after three independent experiments. (b) Wind vane steering regulation on a sailing boat (adapted from ²⁶). At the rear of the boat, an immersed rudder (yellow) serves to steer the boat and an wind vane in the air (green) is sensitive to wind direction. The wind vane is coupled to a trim-tab fixed on the rudder. The rotation of the wind vane/trim-tab, which requires little power, is actuated by the wind, whereas the hydrodynamic coupling between trim-tab and rudder (yellow) induces a strong hydrodynamic torque on the rudder and the required power to turn the boat. (c) Comparative self steering model for a sailing boat and a lymphocyte. (i) A faint external cue, wind or flow (blue arrow), induces a slight rotation of the wind-vane or uropod (green), which (ii) biases the powerful steering machinery (yellow) of the boat (rudder) or of the lymphocyte (the front rear axis of polarization). (iii) The boat or cell turns until the wind vane or uropod is aligned with the external flow and the steering mechanism is back to neutral position.

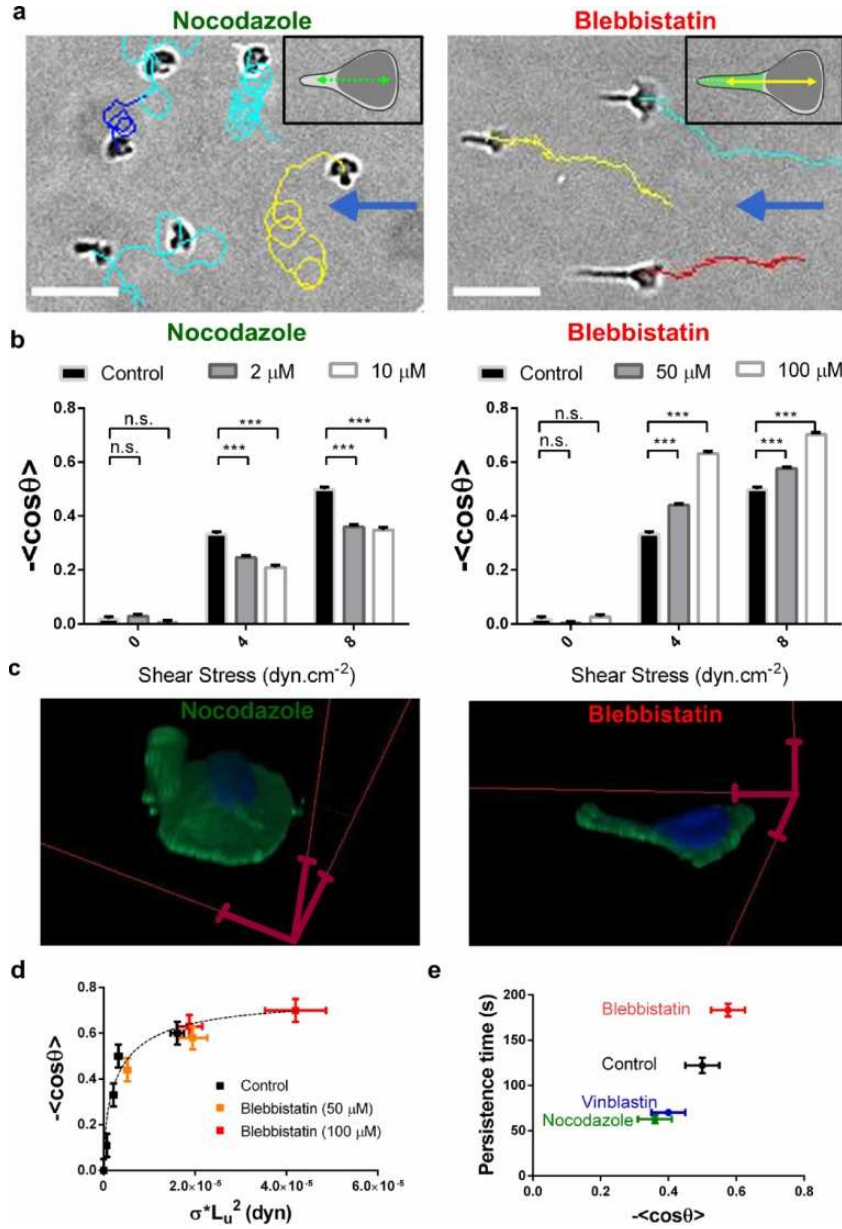


Fig 6. Perturbation of the wind vane self-steering system with inhibitors of microtubules and actomyosin contractility. (a) Cells trajectories superposed to transmission image at a shear stress of 8 dyn.cm⁻², and with nocodazole and blebbistatin at respectively 10 μM and 100 μM. Blue arrows indicate flow direction. Scale bars 50 μm. Inserts in (a) are mechanistic cartoons of nocodazole- and blebbistatine-treated cells with loose transmission mechanism (dotted green arrow, left) and enlarged detection mechanism (green uropod, right). (b) Index of directionality $\langle \cos \theta \rangle$ vs. shear stress. For each condition, data are mean \pm s.e.m of one experiment with $N_{cells} > 100$, representative of $n = 3$ experiments. * $P < 0.05$, ** $P < 0.01$, *** $P < 0.001$ (two tailed unpaired t -test). (c) 3D confocal microscopy images of cells stained for the membrane (green) and the nucleus (blue) in the absence of flow with nocodazole 10 μM (left) and blebbistatin 100 μM (right). Red scale bars 5 μm. (d) Index of directionality $\langle \cos \theta \rangle$ versus shear stress multiplied by the square of the average uropod length $\sigma * L_u^2$ of effector T cells, for control (black dots), and for blebbistatin treatments 50 μM (orange dots) and 100 μM (red dots). All data follow a single master curve (dotted line). Data are mean \pm s.e.m of three independent experiments with $N_{cells} > 20$ per condition. Horizontal errors bars are calculated using s.e.m of L_u . (e) Persistence time of the ballistic regime in the random migration in absence of flow versus the index of directionality $\langle \cos \theta \rangle$ in presence of a flow of 8 dyn.cm⁻², for normal cells and for cells with treatment nocodazole 10 μM, blebbistatin 100 μM, and vinblastin 10 nM. Data are mean \pm s.e.m of three independent experiments with $N_{cells} > 200$ per condition.

MOVIES

Movie 1: Lymphocytes crawling in a flow of changing direction at low magnification. Images sequence of lymphocytes crawling on an ICAM-1/BSA coated glass substrate at a shear stress of 10 dyn.cm^{-2} . The grey arrow indicates the direction of flow, which is from top to bottom in the beginning of the sequence and from right to left in the end. Observation with magnification $\times 20$, one frame acquisition every 20 s, display 10 fps.

Movie 2: Lymphocyte crawling in a flow of changing direction at high magnification. Image sequence of lymphocytes crawling on an ICAM-1/BSA coated glass substrate at a shear stress of 12 dyn.cm^{-2} . The yellow arrow indicates the direction of flow, which is from top to bottom in the beginning of the sequence and from right to left in the end. Observation with magnification $\times 63$, one frame acquisition every 2 s, display 10 fps.

Movie 3: Three dimensional conformation of a crawling T lymphocyte. Confocal microscopy imaging of a T lymphocyte fixed while crawling in the absence of flow on an ICAM-1/BSA coated glass substrate and stained for the membrane (green) and the nucleus (blue).

Movie 4: Adhesion footprint of crawling lymphocytes on an ICAM-1/BSA treated substrate. Movie of superimposed reflection interference contrast microscopy (RICM) and phase contrast images of T lymphocytes crawling under a shear stress of 8 dyn.cm^{-2} . The adhesion zone appears dark on RICM images, which reveals that uropods are non adherent. Arrow indicates direction of flow. One frame acquisition every 20 s, display 5 fps.

Movie 5: Quasi-static regular star conformation of T lymphocytes multiplets attached by their uropod. Bright field movie of a multiplet of $n = 5$ lymphocytes attached by their uropods via anti-ICAM3 coated beads. The multiplet takes a quasi-stable star-like conformation with regular angles of $2\pi/5$. After detachment of a cell, the new multiplet with $n = 4$ stabilizes into a star-like conformation with regular angles of $2\pi/4$ within 50 s. One frame acquisition every 5 s, display 10 fps.

Movie 6: Dynamic reorientation of T lymphocytes in a flow starting from an unstable position. Bright field movie of a T lymphocyte in a right to left flow (white arrow) corresponding to a shear stress of 10 dyn.cm^{-2} , that faces initially downstream due to an attachment of the trailing edge and reorients progressively toward the flow after uropod detachment. One frame acquisition every 10 s, display 10 fps.

Movie 7: Driving a lymphocyte using the uropod as a steering-wheel. Images sequence of a single lymphocyte with a $12 \mu\text{m}$ diameter magnetic bead attached to its uropod and submitted alternatively to hydrodynamic force (blue arrow) pulling the bead to the left and to a magnetic force (red arrow) pulling the bead to the top. The cell is kept immobile in the field of view via a dynamic control of the microscope X-Y stage to maintain the distance between the bead and the magnetic tip constant. Dots indicate the successive relative positions of the cell every 2 s during hydrodynamic (blue dots) and magnetic (red dots) actuation. The trajectory displays

steps with blue horizontal segments and red vertical segments corresponding to the cycles of hydrodynamic and magnetic actuation of 200 pN with 90° angle. Scale bar = 10 µm. One frame acquisition every 10 s, display 10 fps.

Movie 8: Imaging of Calcium signalling in crawling lymphocytes under flow. Relative intracellular internal calcium concentration imaged in crawling lymphocytes labelled with fluo4 PBX at 0.5 µM, and displayed with a pseudo-colour glow scale (red, highest to blue, lowest activity). Flow is null in the beginning of sequence, a white arrow indicating flow direction appears in the sequence when flow is started (corresponding to a shear stress of 8 dyn.cm⁻². Calcium level is unaffected by flow application, but strongly increased upon cell encounters or cell death. Scale bar = 20 µm; sequence is representative of 10 experiments.

Movie 9: Microtubule disruption loosens the transmission of the uropod/wind vane self-steering mechanism. Images sequence of lymphocytes treated with 10 µM of nocodazole and crawling on an ICAM-1/BSA coated glass substrate at a shear stress of 8 dyn.cm⁻². The white arrow indicates the direction of flow. Observation with magnification x20, one frame acquisition every 10 s, display 10 fps.

Movie 10: Three dimensional conformation of a crawling T lymphocyte with nocodazole treatment showing 360° extension of the lamellipod. Confocal microscopy imaging of a T lymphocyte treated with nocodazole at 10 µM, fixed while crawling in the absence of flow on an ICAM-1/BSA coated glass substrate, and stained for the membrane (green) and the nucleus (blue).

Movie 11: Three dimensional conformation of a crawling T lymphocyte with blebbistatin treatment showing strong elongation of the uropod. Confocal microscopy imaging of a T lymphocyte with blebbistatin at 100 µM, fixed while crawling in the absence of flow on an ICAM-1/BSA coated glass substrate, and stained for the membrane (green) and the nucleus (blue).

Movie 12: Stretching the shape of the uropod enhances the efficiency of the uropod/wind vane self-steering mechanism. Images sequence of lymphocytes treated with 100 µM of blebbistatin and crawling on an ICAM-1/BSA coated glass substrate at a shear stress of 8 dyn.cm⁻². The white arrow indicates the direction of flow. Observation with magnification x20, one frame acquisition every 10 s, display 10 fps.

Movie 13: Adhesion footprint of blebbistatin-treated lymphocytes crawling in a flow of changing direction at high magnification. Movie of superimposed reflection interference contrast microscopy (RICM) and phase contrast images of T lymphocytes crawling under a shear stress of 24 dyn.cm⁻² on an ICAM-1/BSA coated glass substrate in presence of 100 µM of blebbistatin at a shear stress of 24 dyn.cm⁻². The adhesion zone appears dark on RICM images, which reveals that uropods are non adherent. The white arrow indicate the direction of flow. Observation with magnification x40, one frame acquisition every 5 s, display 10 fps. Scale bar = 10 µm.

Movie 14: Blebbistatin-treated lymphocytes crawling in a flow of changing direction at low magnification. Image sequence of lymphocytes crawling on an ICAM-1/BSA coated glass substrate in presence of 100 μM of blebbistatin at a shear stress of 24 dyn.cm^{-2} . The white arrow indicates the direction of flow. Observation with magnification $\times 10$, one frame acquisition every 2 s, display 10 fps.

Methods

Flow devices. Devices to change flow direction by 90° were fabricated using standard soft lithography routines¹³. A positive mould was created with SU-8 2100 negative resins (Microchem, USA) on silicon wafers (Siltronic, France), then replicas were moulded in Polydimethylsiloxane (PDMS) elastomer (Sylgard 184, Dow Corning, USA) and sealed on glass coverslips via plasma activation (Harricks plasma, USA). Ports to plug inlet and outlet reservoirs were punched with a 1 mm outer diameter needle. The device is composed of two entries leading to perpendicular channels, and one output. Switching injection from one entry to the other induces a change of flow direction by 90° in the confluence region between the channels connected to the entries. Devices for experiments using magnetic actuation were made of two glass coverslips separated by a 300 μm thick PDMS film and sealed by plasma activation. The channel (3 x 45 mm) was cut in a 300 μm thick PDMS film from Sterne (Cavaillon, France) using a cutting plotter from Graphtec (Yokohama, Japan), and 1 mm diameter holes for entry of fluid in the upper glass coverslip were drilled by sandblasting. The upper face of the device was chosen thin to minimize the distance between the magnetic tweezers tip and the beads in the liquid cell in order to maximize the accessible magnetic actuation force. Flow devices were coated overnight at 4°C with 10 $\mu\text{g/ml}$ human ICAM-1-Fc (R&D Systems, Minneapolis, MN) in PBS (Gibco). Channels were subsequently blocked with 2.5% bovine serum albumin (Axday, Dardilly, France) and 2.5% Pluronic F-108 (BASF, Ludwigshafen, Germany) in PBS (Gibco) for 30 min at room temperature. Channels were rinsed with PBS. Cells were then added in complete culture medium, allowed to equilibrate for 10 min and then rinsed with medium.

Flow control. In the device to change flow direction by 90° , flow rates were controlled via a difference of levels between two fluid reservoirs connected to the inputs and output of the device. An automatic multi-ways valve (Nonapeak, Scivex, Oak Harbour, WA, USA) was inserted between the entry reservoir and the two entries to restrict connection of a single entry at a time to the entry reservoir. Switching the valve from one entry to the other allowed a change of the flow direction in the device in a fraction of second. For all experiment in straight channels on cells with beads attached to their uropod, the flow was controlled using two syringe pumps (Nemesys, Cetoni GmbH, Germany) and two two-way automatic valves assembled in a closed circuit to provide a continuous and unidirectional flow in the channels upon filling/emptying cycles of each syringe.

Microscopic observations. We used a Zeiss Observer Z1 microscope (Carl Zeiss, Oberkochen, Germany) piloted with $\mu\text{Manager}$ ¹⁴ and MATLAB. The microscope was equipped with a CoolSnap HQ CCD camera (Photometrics, Tucson, AZ) and different Zeiss objectives for bright field and Differential Interferential Contrast (DIC) mode (Plan-Apochromat 10x/0.3, 20x/0.8, and 63x/1.4), for Reflection Interference Contrast Microscopy (RICM) mode (Neofluar 63/1.25 antilex), and for Total Internal Reflection Fluorescence (TIRF) mode (100x/1.45). The source was an X-cite 120Q lamp (Exfo, Mississauga, Canada) for bright field, DIC and RICM mode and a laser for TIRF. A narrow band pass filter ($\lambda=546\text{nm} \pm 12\text{nm}$) was used for RICM, whereas the wavelength was of 488 nm for TIRF.

Confocal microscopy was performed on a Leica SP5 confocal equipped with LAS AF Lite Software.

Cells and reagents. Whole blood from healthy adult donors was obtained from the “Etablissement Francais du Sang”. Peripheral blood mononuclear cells (PBMCs) were recovered from the interface of a Ficoll-Paque PLUS (GE Healthcare, Pittsburgh, PA) gradient. The PBMCs were then stimulated for 72 hours with 10 mg/mL phytohemagglutinin-L (PHA-L; Roche Diagnostics, Indianapolis, IN) at 37°C/5% CO₂ and subsequently cultivated in Roswell Park Memorial Institute Medium (RPMI) 1640 supplemented with 25 mM Hepes and 25 mM GlutaMax (Gibco, Carlsbad, CA), 10% fetal calf serum (FCS; Lonza, Basel, Switzerland) in the presence of IL-2 (50 ng/ml; Miltenyi Biotec, Auburn, CA). Cells were typically used 7–10 days after stimulation. At the time of use, the cells were >95% positive for pan-T lymphocyte marker CD3ε and negative for T lymphocyte activation marker CD69 as judged by flow cytometry. Pan-LFA-1 antibody mAb38, was a generous gift of N. Hogg (UK Cancer Research, UK). Alexa 488 labeled goat anti-mouse secondary antibody and FITC labelled Wheat germ agglutinin was from Life Technologies (Carlsbad, CA, USA). Biotinylated anti-ICAM-3 was from AbCAM (Cambridge, UK). Hoechst 3342, vinblastin, and nocadazole was from Sigma Aldrich (St. Louis, MO USA), wortmannin from Calbiochem (San Diego, CA, USA), blebbistatin from Fisher Bioblock Scientific (Illkirch, France), and Fluo-4 PBX Calcium Assay Kit from BDBiosciences (San Jose, CA, USA).

Cell treatments. For fluorescence staining of cells in confocal and TIRF microscopy, cells were allowed to adhere to ICAM-1-Fc coated microfluidic channels for 20 min at 37°C before fixation with 3.5% paraformaldehyde. Samples were subsequently labelled with WGA, mAb38 and/or Hoechst 3342 as per manufacturer’s instructions, and stabilized with ProLong Gold (Life Science Technologies). For experiments with nocadazole and blebbistatin, stock solutions were prepared in dimethyl sulfoxide (DMSO) following manufacturers specification and stored at -20°C and then diluted in culture medium for flow experiments with a DMSO content < 0.5%. Cells were injected in microfluidic channels with culture medium and let settled for 5 min to allow adhesion. Drug solutions were then injected at low shear stress (<1 dyn.cm⁻²) and after a 10 min incubation period, experiments under flow were started keeping the same concentration condition in the flowing fluid. For calcium imaging experiments, cells were first injected in a microfluidic channel with culture medium and let settled for 5 min to allow adhesion, then a BD PBX solution (according to manufacturer instruction) diluted 2000x (~0.5 μM) was injected for 30 min at 37°C in the dark. Cells were finally washed with RPMI medium supplemented with 2% FCS and 10 mM Hepes.

Cell tracking and data analysis. A home-made program was developed with MATLAB software (The Math- Works, Natick, MA) to track migrating cells and analyze their pathway properties¹⁵. In order to get an indication of the amount of movement in a particular direction, we computed the average cosine of the angle, $\langle \cos \theta \rangle$, between this direction and the orientation of the cell path for two positions separated by 50 s. This index is equivalent to the chemotactic index that is usually used to quantify the migration direction relative to gradients of chemotactic factors. The average speed of a cell is calculated as the ratio between the contour length of the total trajectory and the corresponding time of migration.

Magnetic actuation. Magnetic fields were applied with a permanent magnet lying directly on top of the straight channel flow device, or with a custom-made magnetic tweezers set-up positioned in the close vicinity of the flowing channel. We used two types of magnetic beads with diameter 2.8 μm (Dynabeads® M-270 Streptavidin, Invitrogen, Norway) and 12 μm (micromod®, M-Streptavidin 08-19-124). To equip cells uropods with magnetic beads, 10 μL

of streptavidin beads stock solution were washed three times in 100 μ L PBS solution, and 2 μ L of biotinylated anti-ICAM3 antibody was added for 30 min. Beads were then washed three times in PBS solution and finally re-suspended in 100 μ L of culture medium. Cells were injected in the flow devices in complete culture medium, allowed to equilibrate for 10 min at 37°C, before rinsing. The solutions of Ab-coated beads were then injected and allowed to equilibrate with crawling cells for roughly 15min. The beads lying on the lower surface were progressively picked up by crawling cells upon random encounters. When an appropriate number of crawling had picked up a bead and before too many cells had picked up multiple beads, channels were rinsed, which eliminated unattached beads. Samples were imaged with an inverted microscope, whereas the magnetic field source (magnet or tweezers) were positioned above the sample. Flow devices were turned upside-down to minimize the distance between the cells and the magnetic field source (Supplementary Fig. 8), the lowest limit being imposed by the channel ceiling made by a microscope slide of thickness 130 μ m. With magnetic tweezers, the tip was placed at 220 μ m from the magnetic bead attached to a cell and the distance was kept constant during the experiment by maintaining the bead in the centre of the field. The movement of the beads due to the migration of the carrying cell were dynamically compensated by opposite movement of microscope X-Y stage via an automatic regulation code written in Matlab and run using μ Manager interface¹⁴. Movements of the stage were used to reconstruct the migration trajectory of the cell. Calibration of forces on the beads was performed by measuring the velocity of beads in bulk suspension of known viscosity at different positions in the device. For 12 μ m diameter beads, the force applied with the magnetic tweezers was of 120 ± 50 pN, the dispersion being due to the dispersion in diameter and magnetic susceptibility of the beads.

References

1. Huttenlocher, A. & Horwitz, A. R. Integrins in Cell Migration. *Cold Spring Harb. Perspect. Biol.* **3**, (2011).
2. Petri, B., Phillipson, M. & Kubes, P. The physiology of leukocyte recruitment: An in vivo perspective. *J. Immunol.* **180**, 6439–6446 (2008).
3. Bartholomaeus, I. *et al.* Effector T cell interactions with meningeal vascular structures in nascent autoimmune CNS lesions. *Nature* **462**, 94–U104 (2009).
4. Valignat, M.-P., Theodoly, O., Gucciardi, A., Hogg, N. & Lellouch, A. C. T Lymphocytes Orient against the Direction of Fluid Flow during LFA-1-Mediated Migration. *Biophys. J.* **104**, 322–331 (2013).
5. Iijima, M., Huang, Y. E. & Devreotes, P. Temporal and spatial regulation of chemotaxis. *Dev. Cell* **3**, 469–478 (2002).
6. Affolter, M. & Weijer, C. J. Signaling to Cytoskeletal Dynamics during Chemotaxis. *Dev. Cell* **9**, 19–34 (2005).
7. Cai, H. & Devreotes, P. N. Moving in the right direction: How eukaryotic cells migrate along chemical gradients. *Semin. Cell Dev. Biol.* **22**, 834–841 (2011).
8. Sawada, Y. *et al.* Force Sensing by Mechanical Extension of the Src Family Kinase Substrate p130Cas. *Cell* **127**, 1015–1026 (2006).
9. Zaidel-Bar, R., Kam, Z. & Geiger, B. Polarized downregulation of the paxillin-p130(CAS)-Rac1 pathway induced by shear flow. *J. Cell Sci.* **118**, 3997–4007 (2005).
10. Abraham, V., Krishnamurthi, V., Taylor, D. & Lanni, F. The actin-based nanomachine at the leading edge of migrating cells. *Biophys. J.* **77**, 1721–1732 (1999).
11. Sanchez-Madrid, F. & Serrador, J. M. Bringing up the rear: defining the roles of the uropod. *Nat. Rev. Mol. Cell Biol.* **10**, 353–359 (2009).
12. Wright, G. A. *et al.* On-Chip Open Microfluidic Devices for Chemotaxis Studies. *Microsc. Microanal.* **18**, 816–828 (2012).

13. Bairstow, L., Cave, B. M. & Lang, E. D. The Resistance of a Cylinder Moving in a Viscous Fluid. *Philos. Trans. R. Soc. Lond. Ser. Contain. Pap. Math. Phys. Character* **223**, 383–432 (1923).
14. Hogg, N., Patzak, I. & Willenbrock, F. The insider's guide to leukocyte integrin signalling and function. *Nat. Rev. Immunol.* **11**, 416–426 (2011).
15. Ridley, A. J. *et al.* Cell migration: Integrating signals from front to back. *Science* **302**, 1704–1709 (2003).
16. Smith, L. A., Aranda-Espinoza, H., Haun, J. B., Dembo, M. & Hammer, D. A. Neutrophil traction stresses are concentrated in the uropod during migration. *Biophys. J.* **92**, L58–L60 (2007).
17. Goldman, A. J., Cox, R. G. & Brenner, H. Slow viscous motion of a sphere parallel to a plane wall—II Couette flow. *Chem. Eng. Sci.* **22**, 653–660 (1967).
18. Kuras, Z., Yun, Y.-H., Chimote, A. A., Neumeier, L. & Conforti, L. KCa3.1 and TRPM7 Channels at the Uropod Regulate Migration of Activated Human T Cells. *Plos One* **7**, e43859 (2012).
19. Dixit, N., Yamayoshi, I., Nazarian, A. & Simon, S. I. Migrational Guidance of Neutrophils Is Mechanotransduced via High-Affinity LFA-1 and Calcium Flux. *J. Immunol.* **187**, 472–481 (2011).
20. Manahan, C. L., Iglesias, P. A., Long, Y. & Devreotes, P. N. Chemoattractant signaling in *Dictyostelium discoideum*. *Annu. Rev. Cell Dev. Biol.* **20**, 223–253 (2004).
21. Rickert, P., Weiner, O. D., Wang, F., Bourne, H. R. & Servant, G. Leukocytes navigate by compass: roles of PI3K gamma and its lipid products. *Trends Cell Biol.* **10**, 466–473 (2000).
22. Allen, G. M., Mogilner, A. & Theriot, J. A. Electrophoresis of Cellular Membrane Components Creates the Directional Cue Guiding Keratocyte Galvanotaxis. *Curr. Biol.* **23**, 560–568 (2013).
23. Decave, E. *et al.* Shear flow-induced motility of *Dictyostelium discoideum* cells on solid substrate. *J. Cell Sci.* **116**, 4331–4343 (2003).
24. Riviere, C. *et al.* Signaling through the phosphatidylinositol 3-kinase regulates mechanotaxis induced by local low magnetic forces in *Entamoeba histolytica*. *J. Biomech.* **40**, 64–77 (2007).
25. Urbich, C. *et al.* Shear stress-induced endothelial cell migration involves integrin signaling via the fibronectin receptor subunits alpha(5) and beta(1). *Arterioscler. Thromb. Vasc. Biol.* **22**, 69–75 (2002).
26. Moitessier, B. *La longue route*. (Arthaud, 1971).
27. Chichester, F. *Gipsy Moth circles the world*. (Hodder & Stoughton, 1967).
28. Siegrist, S. E. & Doe, C. Q. Microtubule-induced cortical cell polarity. *Genes Dev.* **21**, 483–496 (2007).
29. Xu, J., Wang, F., Keymeulen, A. V., Rentel, M. & Bourne, H. R. Neutrophil microtubules suppress polarity and enhance directional migration. *Proc. Natl. Acad. Sci. U. S. A.* **102**, 6884–6889 (2005).
30. Takesono, A., Heasman, S. J., Wojciak-Stothard, B., Garg, R. & Ridley, A. J. Microtubules Regulate Migratory Polarity through Rho/ROCK Signaling in T Cells. *Plos One* **5**, (2010).
31. Morin, N. A. *et al.* Nonmuscle myosin heavy chain IIA mediates integrin LFA-1 de-adhesion during T lymphocyte migration. *J. Exp. Med.* **205**, 195–205 (2008).
32. Gabriele, S., Benoliel, A.-M., Bongrand, P. & Theodoly, O. Microfluidic Investigation Reveals Distinct Roles for Actin Cytoskeleton and Myosin II Activity in Capillary Leukocyte Trafficking. *Biophys. J.* **96**, 4308–4318 (2009).

Acknowledgements

We thank Pascal Weber and Laurent Limozin for assistance with confocal and TIRF microscopy respectively; Vincent Studer, Igor Ozerov and Frederic Bedu for advice with microfabrication, Yannick Hamon and Julier Treguier for help with calcium experiments. In addition to institutional funds from the CNRS, INSERM and Aix-Marseille Université, this work was funded by grants from the ‘Association pour la Recherche contre le Cancer’, the ‘Fondation de Recherche Médicale’, the ‘CNRS programme Prise de Risques’, and the région PACA France.

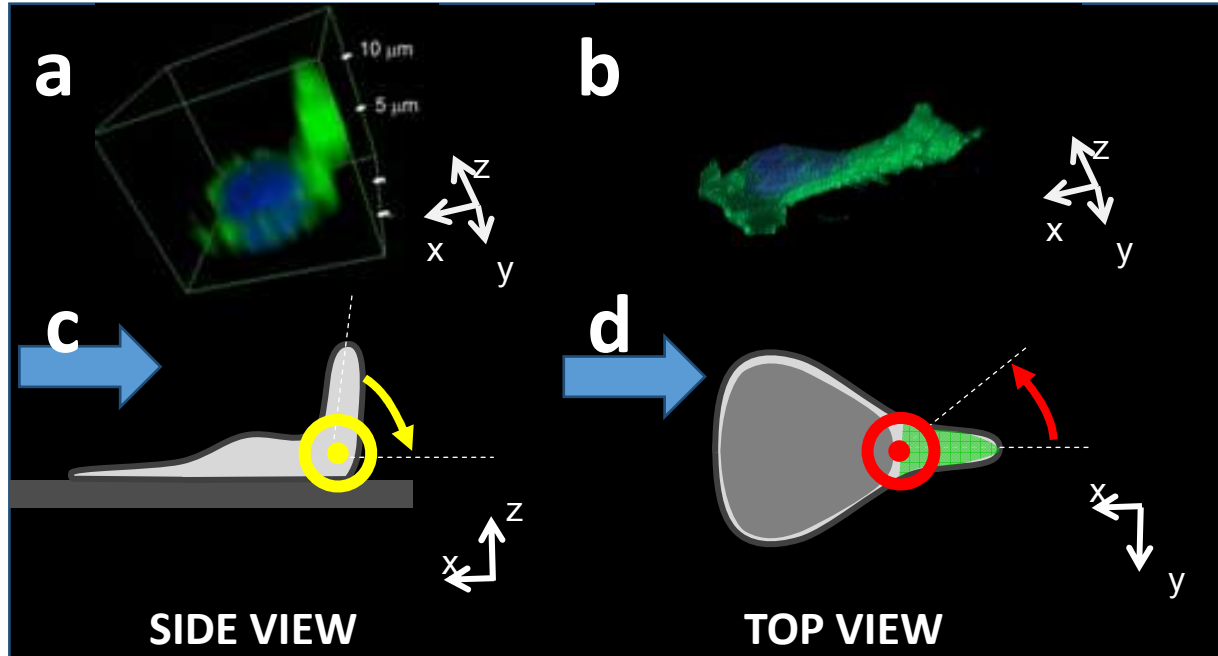
Author contributions

MPV was involved in study design and paper writing, analyzed all data, performed TIRF/confocal imaging and experiments with pharmacological inhibitors; PN performed systematic measurements with flow and magnets, and analyzed data; SC performed part of the experiments with pharmacological inhibitors; ACL was responsible for the cell model and contributed biochemical expertise to key experiments; FG and SH built the magnetic tweezers set-up and performed measurements and calibration; OT designed the study, was involved in all data analysis, developed experiments with beads, fluidic setups, magnetic actuation, microscope feedback control, and wrote the paper. All authors commented on the manuscript.

Supplementary Information

Supplementary Note 1: The uropod has two degrees of freedom of rotation

Hydrodynamic flow may exert torque on the uropod along two perpendicular axis (Supplementary Fig. 1). A first torque acts around an axis parallel to the surface and tends to bend the uropods toward the surface. Confocal images of cells under flow show clearly that the uropod is not erected away from the surface any more but lying alongside the surface (Supplementary Fig. 1b). A second hydrodynamic torque may act on the uropod around an axis perpendicular to the surface that tends to orient the long axis of the uropod in the plane of the substrate with the flow direction, like a wind vane. It is this torque that is relevant in the uropod/wind vane self-steering model. This torque is indeed responsible for the deformation of the rear-front polarization axis of cells (Main text Fig.4c), and in the wind vane self steering model, this bias triggers a new direction of growth for the lamellipod via the maintenance of polarization. Hence, the fact that the uropod is erected away from the surface may increase *sensitivity* to flow but *detection of flow direction* in the wind vane model relies on the orientation of the uropod in the plane of the substrate.

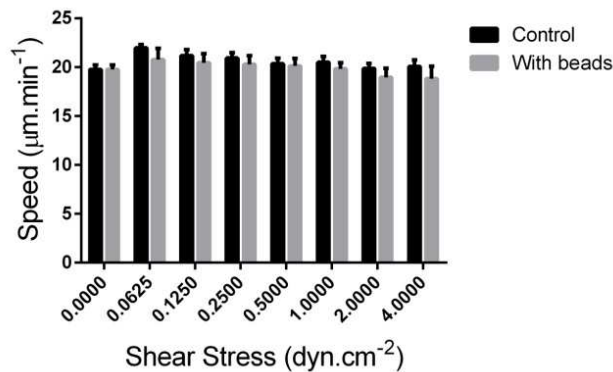


Supplementary Fig. 1: Freedom of rotation of the uropod with flow. (a,b) Erection of uropod versus flow. Confocal images of lymphocytes crawling on a substrate (in the plane $\langle xy \rangle$) with its uropod (a) erected in the z direction perpendicular to the substrate in absence of flow and (b) laying alongside the substrate in presence of a flow of 16 dyn.cm^{-2} . **(c,d) The two axes of rotation of the uropod.** Cartoon of crawling cells viewed (c) from the side (projection in the plane $\langle xz \rangle$) with the axis (yellow) of the torque that pushes the uropod

downwards to the substrate, and **(d)** from the top/bottom (projection in the plane $\langle xy \rangle$) with the axis (red) of the torque that orients the uropod like a wind vane in the plane of the substrate. This latter rotation is the one that is relevant in the uropod/wind vane model.

Supplementary Note 2: Independence of cell speed with attachment of a bead on the uropod

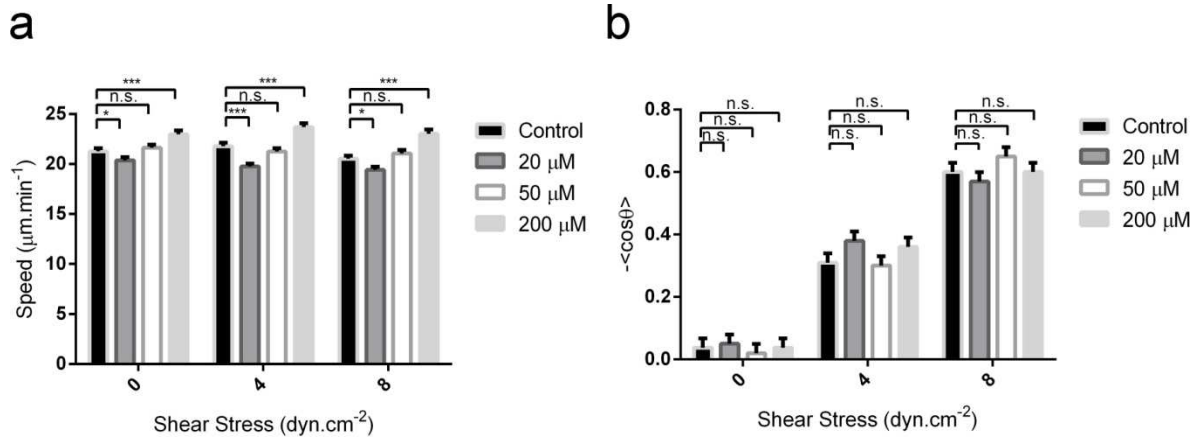
We checked that the average speed of cells was hardly affected by the attachment of a bead to their uropod (Supplementary Fig. 2). This suggests that the attachment of beads does not markedly perturb the normal motility machinery.



Supplementary Fig. 2: Speed of cells bearing a bead on their uropod. Average speed of cells with and without a 12 μm diameter magnetic bead attached to their uropod via ICAM-3 binding. All differences are non significant (two tailed unpaired t -test). Data for each condition were calculated for more than 50 cells over four independent experiments. Error bars indicate \pm s.e.m.

Supplementary Note 3: Inhibition of Calcium channels activity

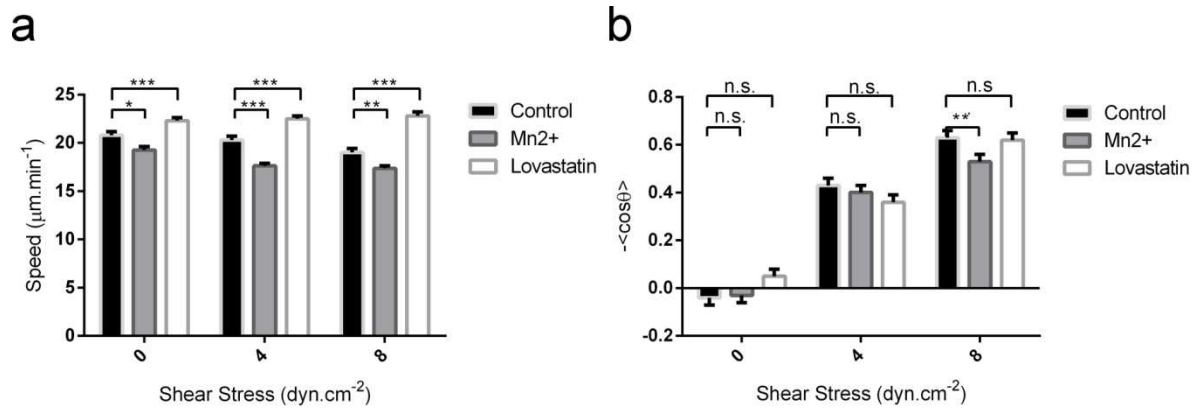
We examined the effect of blocking membrane Ca^{2+} channels using a pharmacological agent of calcium-release-activates (CRAC) channels, SKF-96365^{1,2,3}. CRAC inhibition hardly affects migration speed, as already reported by Kuras et al.², and we found no significant effect on guidance against flow with SKF-96365 concentrations up to 200 μM (Supplementary Fig. 3). These data suggest that CRAC channels, which are preferentially located in the leading edge of lymphocytes, play no central role on the migration and guidance under flow of effector T Cells. Interestingly, Dixit et al.⁴ reported a direct role of CRAC channels in the guidance by flow of non activated neutrophils. Effector lymphocytes and non activated neutrophils seem therefore to behave differently against flow stimuli. However, activated (and polarized) neutrophils, e.g. by fMLP stimulation, have a similar behaviour as effector (and polarized) lymphocytes, as both cell types present no significant intracellular Ca^{2+} influx under flow stimulation. This suggests that the absence of a role for calcium signalling may be a characteristic of polarized leukocytes that are already polarized.



Supplementary Fig. 3: T cell migration characteristics with CRAC inhibitor SKF-96365. (a) Speed and (b) index of directionality $\langle \cos \theta \rangle$ versus shear stress of normal and SKF-treated T cells crawling on ICAM-1 coated substrates. For each condition, data are mean \pm s.e.m of one experiment with $N_{cells} > 200$, representative of $n=3$ experiments. * $P < 0.05$, ** $P < 0.01$, *** $P < 0.001$, two tailed unpaired t -test.

Supplementary Note 4: Modulation of integrins affinity states

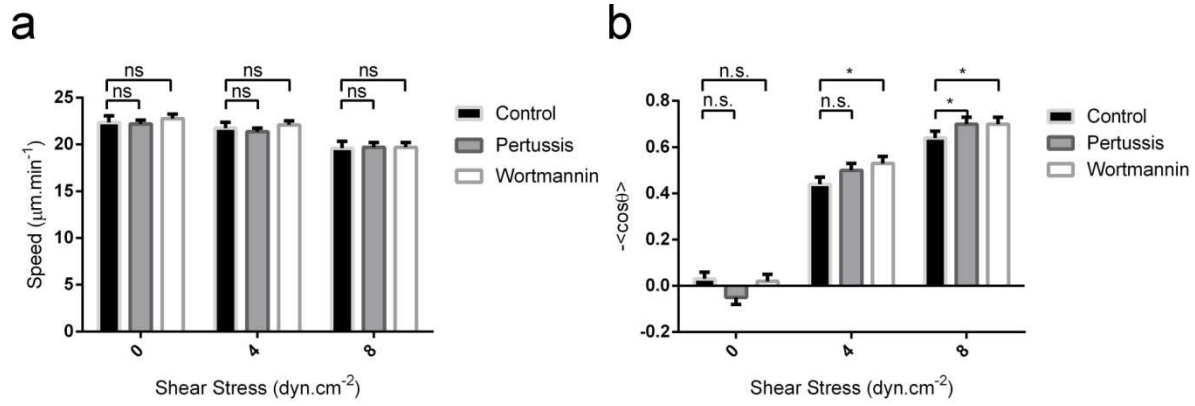
Integrins are part of cell adhesion complexes that may detect *forces*⁵ and are also part of larger scale structures involving stress fibres that may detect *force direction*⁶. For neutrophil guidance under shear stress, evidence of a mechanotransduction mechanism requiring high-affinity LFA-1 adhesion has already been reported⁴. Here, we investigated the role of integrin affinity state on T cell guiding under flow by increasing Mn^{2+} concentration to stabilise integrins in high affinity configuration, and by adding the drug lovastatin to stabilise integrins in intermediate or low affinity configuration. Cells' speed was found to decrease or increase with respectively Mn^{2+} or lovastatin (Supplementary Fig. 4a), which is consistent with an increase or a decrease of adherence respectively⁷. Concerning the guiding under flow, the cells still crawl upstream in presence of both Mn^{2+} and lovastatin (Supplementary Fig. 4b). Upstream crawling is even slightly less pronounced with integrins stabilized in the high affinity state, whereas one may have expected a more pronounced phenotype if high affinity integrins were playing a crucial role in a mechanism involving guidance signalling. Altogether, these results support therefore the idea that mechano-transduction signals mediated by high affinity integrins are not implied in the upstream mechanotaxis mechanism of effector T cells. Moreover, the lower tendency of upstream guiding with Mn^{2+} can well be explained within the uropod/wind vane model. Cells with Mn^{2+} present indeed an increase of adherence of the uropod, which directly perturbs their capacity to orient in the flow like a wind vane.



Supplementary Fig. 4: T cell migration characteristics vs. perturbations of integrins affinity. (a) Speed and (b) index of directionality $\langle \cos \theta \rangle$ versus shear stress of control T cells and T cells in presence of excess Mn^{2+} , which stabilizes integrins in high affinity configuration and lovastatin, which stabilises integrins in intermediate or low affinity configuration. For each condition, data are mean \pm s.e.m of one experiment with $N_{\text{cells}} > 250$, representative of $n=3$ experiments. * $P < 0.05$, ** $P < 0.01$, *** $P < 0.001$, two tailed unpaired t -test.

Supplementary Note 5: Inhibition of PI(3)K and receptor–G-protein interactions

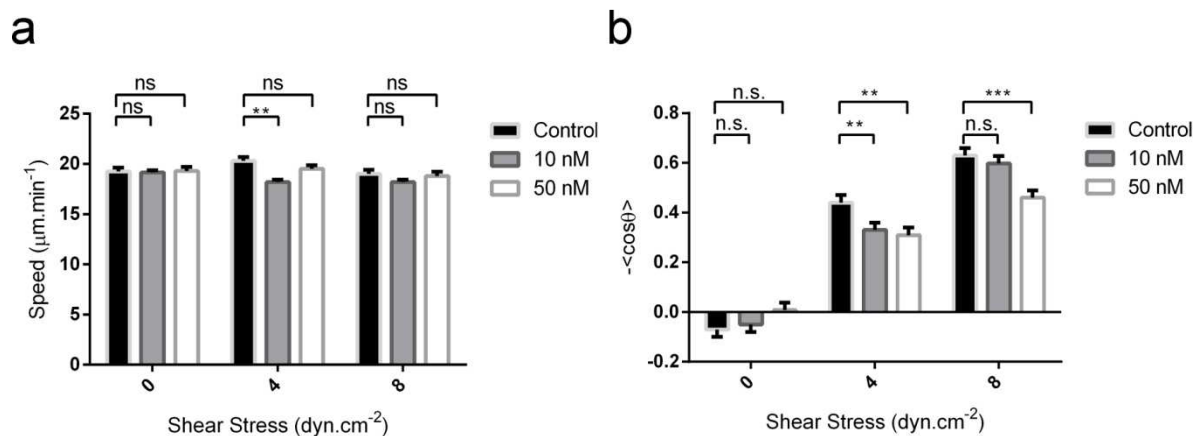
The non-selective PI(3)K inhibitor, wortmannin, has been reported to induce deficiencies in the chemotaxis of mammalian neutrophils⁸ and in mechanotaxis of *Entamoeba histolytica*⁹. We performed migration experiments under flow with effector T cells using similar wortmannin concentrations, and found no major effect on the upstream migration phenotype of T cells (Supplementary Fig. 5). This result comforts the model that a specific signalling route may not be involved in the T cell upstream mechanotaxis phenomenon. The lack of involvement of PI(3)K in effector T cell upstream mechanotaxis supports strongly the proposition of a passive or non specific self-steering mechanism to the external stimulus. Let us note however that this result it cannot be taken as a definitive argument because some guiding phenomena, such as neutrophils chemotaxis that undoubtedly rely on an active mechanism specific to the external cue are functional without the help of PI(3)K activity¹⁰. We then used pertussis toxin (PTX) to inhibit receptor–G-protein interactions and found no effect on speed and orientation of effector T cells under flow (Supplementary Fig. 5). Therefore signalling through heterotrimeric G-proteins, required for many leucocyte chemokine receptors, is not involved in T cell upstream mechanotaxis.



Supplementary Fig. 5: T cell migration characteristics with inhibitor of PI(3)K and G-protein receptors. (a) Speed and (b) index of directionality $\langle \cos \theta \rangle$ versus shear stress of control T cells and T cells in presence of pertussis toxin at 4 nM, which inhibits receptor-G-protein interactions, and wortmannin at 100 nM, which inhibits PI(3)K kinase. For each condition, data are mean \pm s.e.m of one experiment with $N_{cells} > 100$, representative of n=3 experiments. * $P < 0.05$, two tailed unpaired t -test.

Supplementary Note 6: Inhibition of microtubules with vinblastin

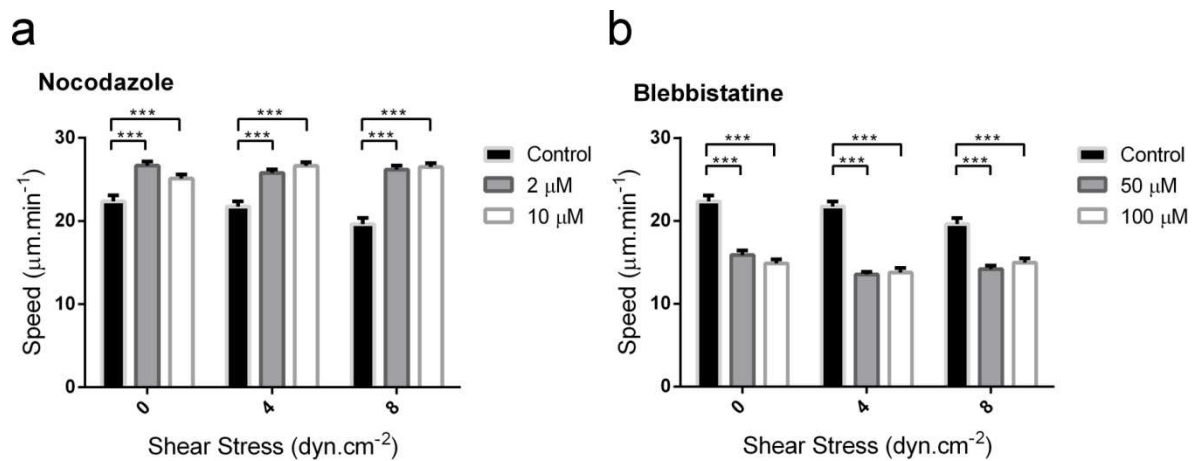
We used another specific inhibitor of tubulin polymerisation¹¹, vinblastin, to strengthen the investigation of microtubule destabilization on T cell migration under flow (Supplementary Fig. 6). Vinblastin had no effect on the speed of T cell with or without flow, whereas a net decrease of orientation under flow was detected with increasing vinblastin concentration. This latter result is similar to the behaviour observed with nocodazole, which further supports the idea that the destabilization of microtubules decreases the efficiency of the upstream mechanotaxis mechanism. In our model of passive uropod wind vane self-steering mechanism, this effect is directly linked to the decrease of the rear-front axis polarization, and therefore to the transmission of the flow direction « detection » by the uropod/wind vane into an upstream direction of migration.



Supplementary Fig. 6: T cell migration characteristics with microtubule polymerisation inhibitor by vinblastin. (a) Speed and (b) index of directionality $\langle \cos \theta \rangle$ versus shear stress of control T cells and T cells in presence of vinblastin. For each condition, data are mean \pm s.e.m of one experiment with $N_{cells} > 250$, representative of n=3 experiments. * $P < 0.05$, ** $P < 0.01$, *** $P < 0.001$, two tailed unpaired t -test.

Supplementary Note 7: Effect of blebbistatin and nocodazole on cell speed

Nocodazole and blebbistatin have been found to respectively increase and decrease the average speed of crawling T cells (**Error! Reference source not found.**). A similar effect with nocodazole was previously attributed to the overactivation of RhoA in the cell rear induced by microtubules depolymerisation¹². Conversely, blebbistatin, was found in the same study to stabilize microtubules against depolymerization, which is consistent with an opposite effect of blebbistatin on speed as compared to nocodazole. However, better understanding of the effect of nocodazole and blebbistatin on T cells speed would deserve further analysis, which is out of the scope of the present paper.

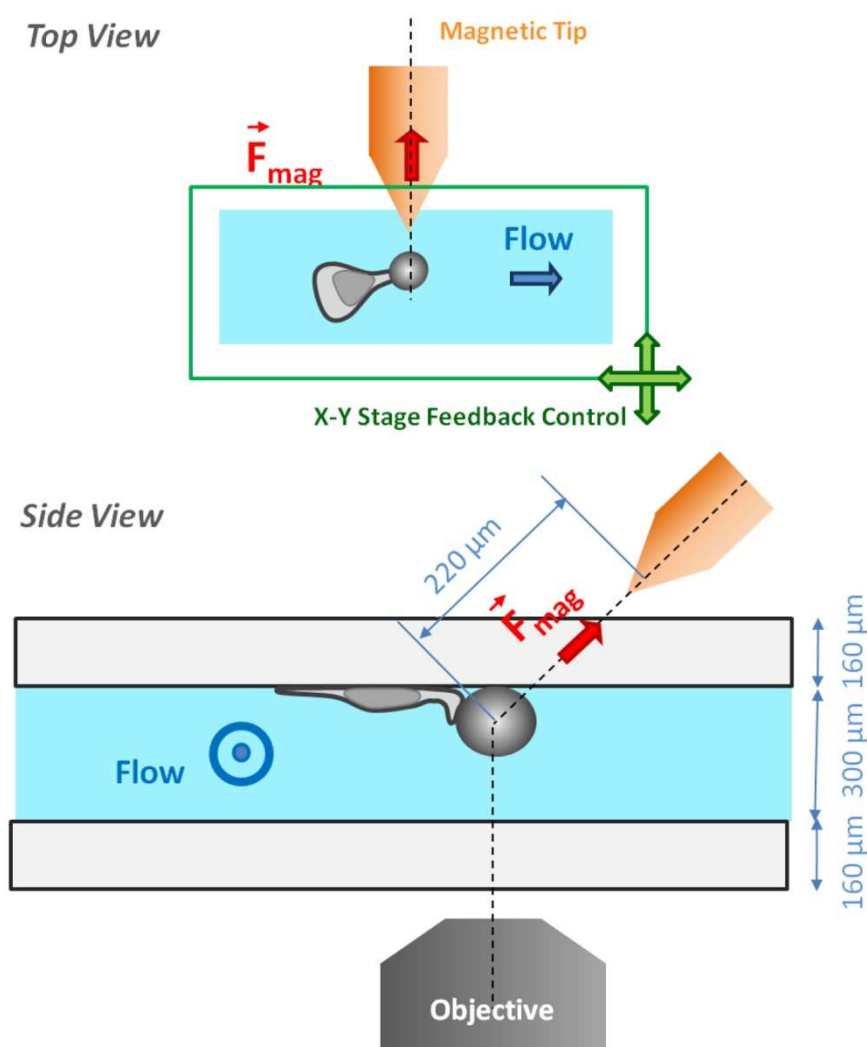


Supplementary Fig. 7: Effect of nocodazole and blebbistatin on cell speed. Speed versus shear stress of control T cells and T cells in presence of (a) nocodazole, which destabilizes microtubules, and (b) blebbistatin, which inhibits acto-myosin contractility. For each condition, data are mean \pm s.e.m of one experiment with $N_{\text{cells}} > 100$, representative of $n=3$ experiments. *** $P < 0.001$, two tailed unpaired t -test.

Supplementary Methods

Reagents. Lovastatin and SKF-96365 was from Sigma Aldrich (St. Louis, MO USA), and wortmaninn from Calbiochem (SanDiego, CA, USA)

Magnetic actuation experiments. Samples were imaged with an inverted microscope, with the objective below the flow device, whereas the magnetic field source (magnet or tweezers) were positioned above the flow device. Flow devices were turned upside-down to minimize the distance between the cells and the magnetic field source (Supplementary Fig. 8), the lowest limit being imposed by the channel ceiling made by a microscope slide of thickness $130\ \mu\text{m}$. Magnetic fields applied with magnetic tweezers were performed on a custom-made set-up. The tip was placed at $220\ \mu\text{m}$ from the magnetic bead attached to a cell and the distance was kept constant during the experiment by maintaining the bead in the centre of the field. The movement of the beads due to the migration of the carrying cell were dynamically compensated by opposite movement of microscope X-Y stage via an automatic regulation code.



Supplementary Fig. 8: Experimental set-up for magnetic actuation experiments. Flow devices made of two glass coverslips separated by $300\ \mu\text{m}$ were used in magnetic actuation

experiments, with microscopic observations made from below and magnetic actuation from above (Side view). Cells were deposited on the ceiling of the devices in order to minimize the distance between the cells and the magnetic field source. A Matlab code and live imaging with a long working distance objective (x20) were used to control the X-Y stage and maintain dynamically the cell in the centre of the field of view (Top view). The magnetic tweezers tip, positioned and maintained at 220 μm from the magnetic bead attached to the cell of interest, applies a constant magnetic force during cell displacement. Hydrodynamic flow in the channel was controlled with a syringe pump, so that in the plane of cellular displacement, the hydrodynamic and magnetic forces on the bead had perpendicular directions.

Supplementary References

1. Feske, S. Calcium signalling in lymphocyte activation and disease. *Nat. Rev. Immunol.* **7**, 690–702 (2007).
2. Kuras, Z., Yun, Y.-H., Chimote, A. A., Neumeier, L. & Conforti, L. KCa3.1 and TRPM7 Channels at the Uropod Regulate Migration of Activated Human T Cells. *Plos One* **7**, e43859 (2012).
3. Svensson, L. *et al.* Calpain 2 Controls Turnover of LFA-1 Adhesions on Migrating T Lymphocytes. *Plos One* **5**, e15090 (2010).
4. Dixit, N., Yamayoshi, I., Nazarian, A. & Simon, S. I. Migrational Guidance of Neutrophils Is Mechanotransduced via High-Affinity LFA-1 and Calcium Flux. *J. Immunol.* **187**, 472–481 (2011).
5. Sawada, Y. *et al.* Force Sensing by Mechanical Extension of the Src Family Kinase Substrate p130Cas. *Cell* **127**, 1015–1026 (2006).
6. Zaidel-Bar, R., Kam, Z. & Geiger, B. Polarized downregulation of the paxillin-p130(CAS)-Rac1 pathway induced by shear flow. *J. Cell Sci.* **118**, 3997–4007 (2005).
7. Laemmermann, T. & Sixt, M. Mechanical modes of ‘amoeboid’ cell migration. *Curr. Opin. Cell Biol.* **21**, 636–644 (2009).
8. Wang, F. *et al.* Lipid products of PI(3)Ks maintain persistent cell polarity and directed motility in neutrophils. *Nat. Cell Biol.* **4**, 513–518 (2002).
9. Riviere, C. *et al.* Signaling through the phosphatidylinositol 3-kinase regulates mechanotaxis induced by local low magnetic forces in *Entamoeba histolytica*. *J. Biomech.* **40**, 64–77 (2007).
10. Fergus, G. J. *et al.* PI(3)K gamma has an important context-dependent role in neutrophil chemokinesis. *Nat. Cell Biol.* **9**, 86–U109 (2007).
11. Gigant, B. *et al.* Structural basis for the regulation of tubulin by vinblastine. *Nature* **435**, 519–522 (2005).
12. Takesono, A., Heasman, S. J., Wojciak-Stothard, B., Garg, R. & Ridley, A. J. Microtubules Regulate Migratory Polarity through Rho/ROCK Signaling in T Cells. *Plos One* **5**, (2010).
13. Ng, J. M. K., Gitlin, I., Stroock, A. D. & Whitesides, G. M. Components for integrated poly(dimethylsiloxane) microfluidic systems. *Electrophoresis* 3461–3473 (2002).
14. Edelstein, A., Amodaj, N., Hoover, K., Vale, R. & Stuurman, N. in *Curr. Protoc. Mol. Biol.* (Ausubel, F. M. *et al.*) (John Wiley & Sons, Inc., 2010). at <<http://doi.wiley.com/10.1002/0471142727.mb1420s92>>
15. Valignat, M.-P., Theodoly, O., Gucciardi, A., Hogg, N. & Lellouch, A. C. T Lymphocytes Orient against the Direction of Fluid Flow during LFA-1-Mediated Migration. *Biophys. J.* **104**, 322–331 (2013).